RESEARCH PAPER

Energy-based evaluation of undrained cyclic behavior of marine soft clay under multidirectional simple shear stress paths

Hongxu Jin[1] · Lin Guo[2] · Honglei Sun[1] · Tingyu Wu[1] · Li Shi[1] 🆔 · Yuanqiang Cai[1]

Abstract
During the service life of marine structures, environmental loads, such as earthquakes and ocean wave storms, may exert dynamic shear stresses of different amplitudes and orientations in the foundation soil. To investigate the undrained cyclic behavior of marine soft clay under a complex shear stress state, a laboratory study was performed on remolded clay specimens using a variable-direction dynamic cyclic simple shear system, through which two mutually perpendicular shear stresses can be simultaneously applied to the specimen within the horizontal x–y plane. Stress paths of linear, circular, and elliptical patterns were obtained by adjusting the amplitude ratio (η) between the two cyclic shear stresses and applied to investigate the undrained behavior of soft clay. The undrained cyclic responses of the clay specimens were presented and then analyzed from the viewpoint of energy dissipation. A strain-softening phenomenon was observed when the cyclic effective stress path reached the failure line determined by the monotonic test. The cyclic strength of clay subjected to multidirectional cyclic shear stresses (i.e., circular and elliptical stress paths) was 0.775^{η} times that under unidirectional shear stress (i.e., linear stress path). The coupling effects of CSR and η on the cyclic strength and accumulation of residual pore water pressure can be uniformly correlated to energy dissipation.

Keywords Cyclic shear strength · Dissipated energy · Marine soft clay · Multidirectional loading · Pore water pressure · Simple shear tests

1 Introduction

Many marine structures such as anchors, offshore wind turbines, and oil/gas platforms are founded on marine clay sediments. During the service life of these structures, operational vibrations of the superstructure and environmental loads from storm waves, earthquakes, and currents may apply cyclic loads of different amplitudes and orientations to the foundation soil. Compared with unidirectional cyclic loading, it has been reported that the residual deformation and associated failure probability of the foundation soil can be amplified when subjected to

multidirectional cyclic loading [15, 29, 35–37, 39]. Accordingly, it is important to understand the multidirectional cyclic behavior of marine soft clay to ensure the functionality and safety of the marine structures.

Over the past few decades, extensive laboratory tests with unidirectional cyclic loading have been performed to study the cyclic behavior of soft clay, for example, triaxial tests [12, 47] and simple shear tests [7, 24]. In the course of storm waves or earthquakes, the cyclic shear strength of clay is a key parameter in the design of clay-based engineering installations. A contour diagram framework on cyclic strength of clay has been proposed by Andersen [4, 5] for unidirectional cyclic loading, where the cyclic stress ratio and number of cycles to cyclic failure are two key parameters. Compared to the monotonic strength of soil, which can be solely represented by stress, the cyclic strength must be described by a combination of the cyclic stress ratio (CSR) and number of cycles required for the specimen to reach failure (N_f); in other words, the cyclic strength is usually defined as the CSR required to reach

✉ Li Shi
  lishi@zjut.edu.cn

1 College of Civil Engineering, Zhejiang University of Technology, Hangzhou 310014, People's Republic of China

2 College of Architecture and Civil Engineering, Wenzhou University, Chashan University Town, Wenzhou 325035, People's Republic of China

cyclic failure in a specified number of loading cycles. N_f is used to evaluate the magnitude of the environmental load in engineering. For instance, N_f was 15 and 30 cycles, which can simulate earthquakes with magnitudes 7.5 and 8.5, respectively [15]. A criterion is needed to judge whether the specimen reaches cyclic failure; however, different choices of failure criteria exist in the literature. Lee [18] conducted a series of cyclic triaxial tests on two types of sensitive undisturbed clay and indicated that a shear failure surface would form in both high- and low-sensitivity clay specimens when the shear strain reaches 4–6% and 2–3%, respectively. Thus, a single-amplitude strain of 3% was considered as the failure criterion for the cyclic deformation of the clay. However, criteria based on different levels of shear strains, for example, 1%, 5%, 10%, and 15%, also exist in the literature [14, 47]. Alternatively, the failure criterion can be based on the effective stress. For example, Malek et al. [24] proposed that a clay specimen is in a failure state when the cyclic effective stress path reaches the failure envelope determined in monotonic tests. Because the pore water pressure response can be reflected in the undrained cyclic stress path, the effective stress-based criterion can also be considered as a pore water pressure-based criterion. It has been frequently observed in laboratory tests [19] that clay specimens collapse in a relatively short period once the amplitude of shear strain is larger than that corresponding to the inflection of the shear strain–cycling number curve. Therefore, Li et al. [19] proposed that the inflection of the curve of single-amplitude shear strain versus the number of cycles can be considered as a distinct sign of cyclic failure. Its emergence can also be considered a suitable failure criterion for clays. It can be seen from the above that no consensus has been reached on suitable criteria for judging the cyclic failure of soft clay.

As fueled by the advancement of bidirectional loading test apparatus, several studies have been conducted to investigate the multidirectional cyclic behavior of soft clay. Gu et al. [10] studied the undrained cyclic behavior of soft clay using cyclic triaxial tests with a variable confining pressure. The test results showed that the excess pore water pressure, cyclic axial strain, and cyclic strength were significantly influenced by the cyclic confining pressure. Matsuda et al. [27] performed a series of multidirectional simple shear tests in a strain-controlled manner to investigate the cyclic behavior of clay, in which cyclic shear strains with the same amplitude but different phases were applied to the specimen from two perpendicular directions in the horizontal plane. It is shown that the excess pore water pressure and post-cyclic consolidation deformation induced by multidirectional cyclic shear are larger than those generated by the unidirectional one of the same shear-strain amplitude and loading cycles. To present the

combined effects of multidirectional cyclic loadings, the concept of dissipated energy, determined from the hysteretic loops of stress–strain, has been proposed and applied. This method was first introduced by Liang et al. [22] to assess the liquefaction potential of sand under complex random cyclic loading conditions. Because the dissipated energy reflects the damage to the soil skeleton when subjected to external cyclic loading [28], it has been applied in extensive laboratory studies to quantify the influences of key factors, including the effective confining pressure [17], relative density [9], consolidation stress ratio [45], and loading waveform [31] on the cyclic strength and pore water pressure responses of soils. In particular, the accumulation of dissipated energy can be mathematically related to the residual pore water pressure, which can be used to numerically predict the soil response [9, 33]. In view of the above, the effects of the phase difference of multidirectional shear loadings and the energy dissipation associated with unidirectional cyclic loading have been reported. However, the effects of the amplitude differences of multidirectional shear stresses on the cyclic responses, let alone interpretation from the perspective of energy dissipation, remain untouched in the literature, which motivates the present study.

In this study, the influences of multidirectional shearing on the cyclic behavior of soft marine clay were investigated using a variable-direction dynamic cyclic simple shear system. Four series of laboratory tests with different loading amplitudes and stress path patterns were designed and performed. Cyclic results, including the effective stress path, shear strain, cyclic strength, and pore water pressure were presented and analyzed. The characteristics of clay specimens under multidirectional shear loading were revealed by comparison with the unidirectional loading case. The concept of dissipated energy was adopted to quantify the cyclic shear strength and pore water pressure generation of soft clay under multidirectional cyclic shear stress paths. Finally, two criteria for cyclic failure and their influence on evaluating the cyclic strength and pore water pressure of clay specimens were discussed.

2 Materials and experimental methods

2.1 Test materials

The soil used in the present study was soft clay obtained from Wenzhou, which is characterized by its high water content, low permeability, high compressibility, and low bearing capacity [11, 41]. Remolded samples were used because undisturbed uniform soft clay samples are very difficult to obtain. The remolded soft clay was prepared using a slurry consolidation method. The clay blocks

sampled from the field were first dried in an oven, and then ground to a powder using a crushing machine. The clay powders were mixed with de-aired water to obtain a slurry with a water content of 80% ($\approx 1.33 w_L$, where w_L represents the liquid limit). The slurry was slowly poured into a large consolidation apparatus with a diameter of 300 mm and height of 400 mm. Vertical consolidation pressures were applied step by step in the sequence of 12.5 kPa, 25 kPa, 50 kPa, and a final pressure of 100 kPa. The consolidation process was complete when the consolidation settlement reached a steady value at each consolidation pressure level. More specific information regarding the remolded clay preparation process can be found in Hu et al. [13] and Wang et al. [43]. The basic index characteristics of the soft clay samples are summarized in Table 1.

2.2 Test apparatus and procedures

This study employed a variable-direction dynamic cyclic simple shear (VDDCSS) system. As shown in Fig. 1, the system consists of three encoder-controlled high-precision actuators. The axial actuator can exert a vertical force. The two horizontal actuators can simultaneously exert horizontal forces. More specific information regarding this apparatus can be found in the work of Li et al. [20] and Jin and Guo [15].

Cylindrical specimens with a diameter of 50 mm and height of 20 mm were trimmed from the remolded soft clay block. The prepared clay specimen was then placed in a shear box, as shown in Fig. 2. A stack of low-friction Teflon-coated rings was placed outside the membrane of the specimen. Because the radial stiffness of the rings is sufficiently high, K_0 conditions of the specimen can be ensured during the consolidation and shearing tests. The stack of rings, each of thickness 1 mm, offers flexibility in developing shearing failure in the specimen along the weakest horizontal surface, which should be deemed as an improvement over the pre-set shearing surface scenario

Table 1 Index properties of remolded soft clay

Index properties	Value
Specific gravity, G_s	2.71
Initial water content, w (%)	43–45
Initial density, ρ_0 (g/cm³)	1.72–1.76
Initial void ratio, e_0	1.19–1.23
Degree of saturation, S_r (%)	97.9–99.1
Liquid limit, w_L (%)	60
Plasticity index, I_p	32
Clay fraction (%)	41
Silt fraction (%)	55

involved in the conventional direct shear test. After placing the shear box at the base of the VDDCSS testing apparatus, an initial vertical consolidation stress of 100 kPa was applied. When the consolidation process was completed, a series of simple shear tests were carried out under a constant volume condition. The variations in the vertical stress ($\Delta\sigma_v$) required to keep constant volume throughout a simple shear test are equal to the measured pore pressures (Δu) in an undrained simple shear test for clay [1, 2, 8]. Throughout the consequential stages of specimen preparation, consolidation and cyclic shearing, no back pressure was applied; therefore, the specimens remained below 100% saturation. However, a degree of saturation (S_r) greater than 97% can still be guaranteed, as shown in Table 1. Notably, the degree of saturation does not affect the mechanical response of soils provided the matric suction is small, and the constant volume condition is satisfied [3, 38]. Thus, the non-fully saturated condition should not be deemed as a drawback in our test.

The two horizontal actuators provide cyclic forces with the same cycling frequency; however, their amplitudes and phases can be different. When only one horizontal actuator is activated (e.g., the one along the x–direction), a unidirectional cyclic loading condition can be achieved, whose typical waveform is given in Fig. 3(a). The shear stress path is linear (Fig. 4). The typical waveforms with a phase difference of 90° when the two actuators work simultaneously are presented in Fig. 3(b). When the two horizontal forces have the same and different amplitudes, the cyclic shear paths are circular and elliptical, respectively, in the horizontal plane, as shown in Fig. 4. The 90° phase difference between the two cyclic shear stresses is chosen because it serves as the most unfavorable loading condition for cyclic behavior of clay specimens when compared to other phase differences (e.g., 20°, 45°, 70°, etc.) [23, 26]. In this study, the cycling frequency of the horizontal loading was taken as the typical frequency of wave loading, that is, 0.1 Hz [4, 40]. A low cycling frequency is also favorable for the reliability of the pore water pressure measurement of the specimen and for the precise control of cyclic stress [26].

By varying amplitudes τ_x and τ_y of the two cyclic shear stresses, different loading conditions can be established to perform the undrained cyclic simple shear tests, as summarized in Table 2. To facilitate the description, the shear stress ratio η is defined as the amplitude ratio between the two cyclic stresses, that is, $\eta = \tau_y/\tau_x$. The cyclic stress ratio CSR is defined as the ratio of τ_x to σ'_{v0} (i.e., CSR = τ_x/σ'_{v0}), where σ'_{v0} denotes the vertical consolidation stress. N_f denotes the number of cycles to failure of the specimen. The failure criteria will be discussed in the following sections.
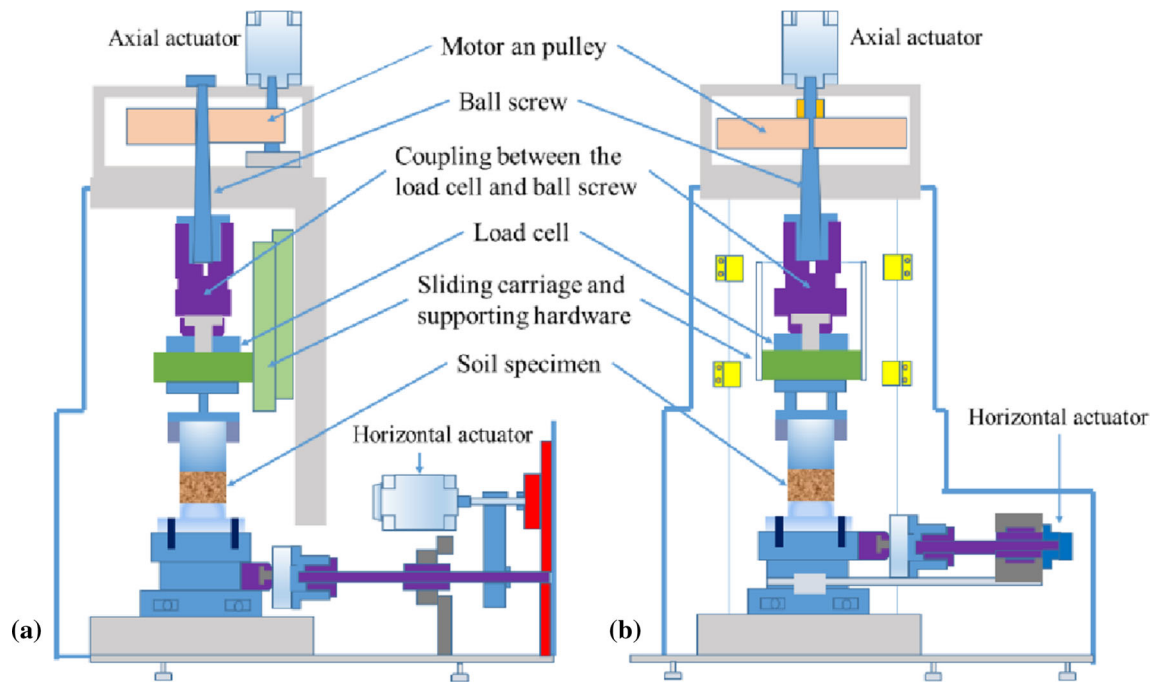
Fig. 1 Schematic of variable-direction dynamic cyclic simple shear (VDDCSS) system in **a** x–z plane and **b** y–z plane
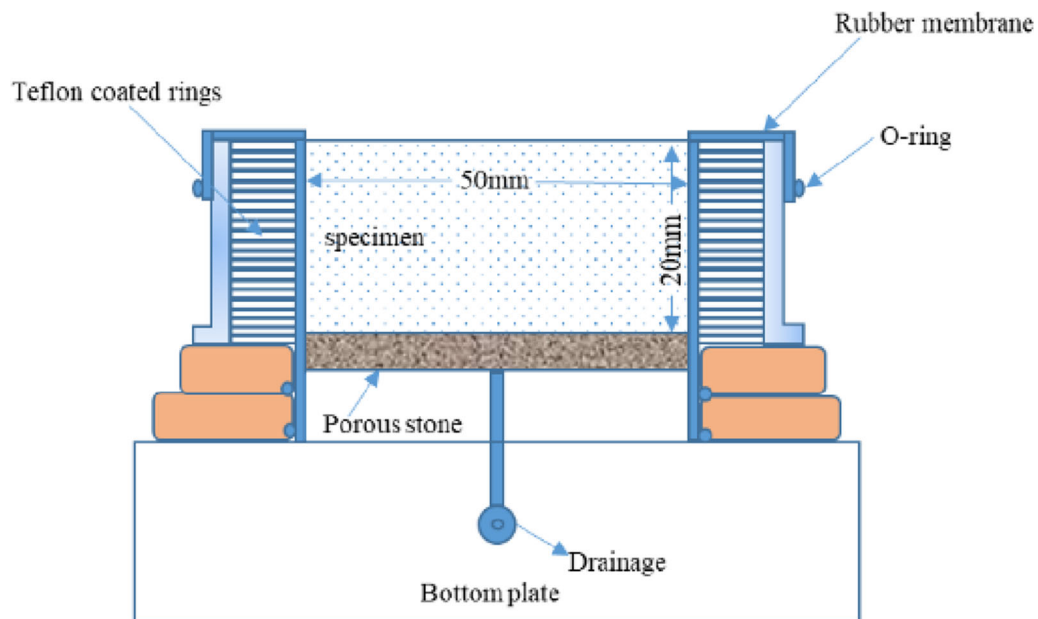

Fig. 2 Schematic of test specimen in the shear box

Four test series were designed in this study. Series I and II are associated with unidirectional ($\eta = 0$) and equal-magnitude multidirectional ($\eta = 1$) loading conditions, respectively. To investigate the effects of η on the cyclic behavior of soft clay, the Series III tests are conducted under cyclic loadings of the same CSR and different η. The combinations of CSR and η associated with Series IV are set such that they are different from those of the remaining test series. In this way, the results from Series IV can help verify the empirical laws established based on test Series I–III.
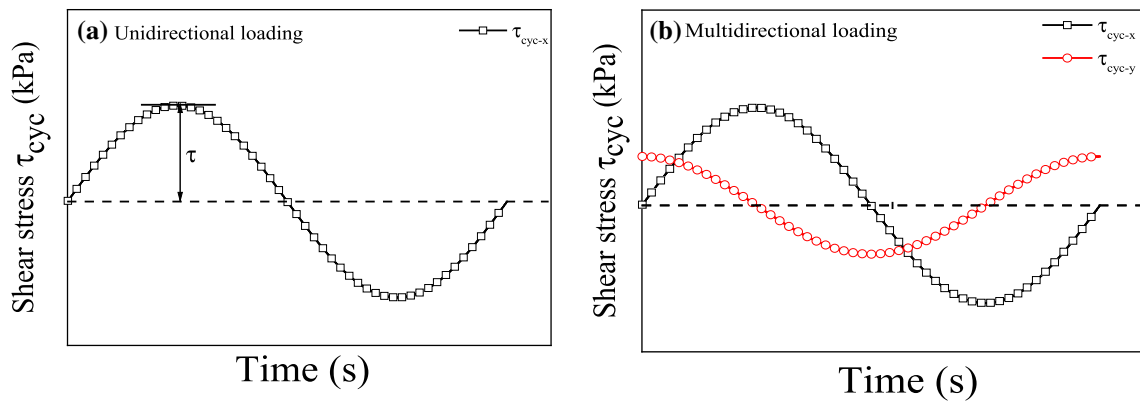
Fig. 3 Schematic of cyclic shear stresses **a** unidirectional loading; **b** multidirectional loading
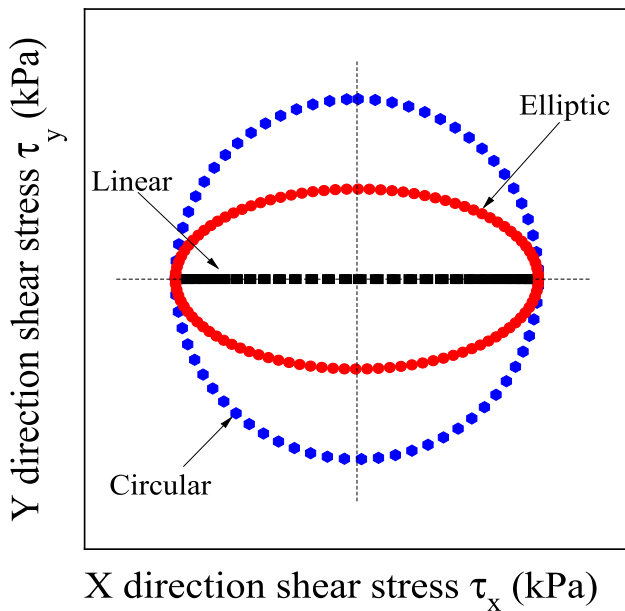

Fig. 4 Schematic of cyclic shear stress in unidirectional and multidirectional cyclic loading conditions

Table 2 Summary list of undrained cyclic simple shear tests

Series	No. of tests	σ'_{v0} (kPa)	τ_x (kPa)	τ_y (kPa)	CSR = τ_x/σ'_{v0}	$\eta = \tau_y/\tau_x$	N_f
I	L1	100	15	0	0.15	0	255
	L2	100	20	0	0.20	0	35
	L3	100	25	0	0.25	0	7
	L4	100	30	0	0.30	0	3
II	C1	100	14	14	0.14	1	78
	C2	100	15	15	0.15	1	36
	C3	100	18	18	0.18	1	17
	C4	100	20	20	0.20	1	7
	C5	100	25	25	0.25	1	2
III	L2	100	20	0	0.20	0	35
	E1	100	20	6	0.20	0.3	24
	E2	100	20	14	0.20	0.7	11
	C4	100	20	20	0.20	1	7
IV	E3	100	16.5	11.5	0.165	0.7	44
	E4	100	18	9	0.180	0.5	34
	E5	100	23.8	7.2	0.238	0.3	7

L: linear stress path, E: elliptical stress path, C: circular stress path

3 Monotonic shear test results

Before performing the cyclic shearing test, the clay specimen is sheared monotonically to evaluate its strength characteristic. Two consolidation stresses were considered: $\sigma_{v0} = 100$ kPa and 200 kPa. After consolidation, the specimen was sheared monotonically at a shear rate of 0.05%/min under the undrained condition. The test results for the stress–strain relationship and effective stress path are presented in Fig. 5. It can be observed that the undrained shear stress (τ) increases with the shear strain (γ) before the specimen reaches the peak shear strength, and then τ decreases slightly in the subsequent shear process. The peak strength increases with the consolidation stress. Excess pore water pressure generates during the shearing of the clay specimen. Thus, a decrease in the vertical effective

stress is observed in Fig. 5(b). A failure line (FL) can be constructed by connecting the peak strength and origin of the stress space, as indicated in Fig. 5b. The slope of the failure line is determined to be $\tau/\sigma_v = 1/1.7$.

4 Representative cyclic responses

For the Series I test, representative results on the effective stress path, stress–strain curve, and development of cyclic shear strain (γ_{cyc}) and double-amplitude shear strain (γ_{DA}) are presented in Fig. 6 for test No. L2, i.e., CSR = 0.2. The effective vertical stress (σ'_v) decreases drastically in the first two cycles because pore water pressure generates.
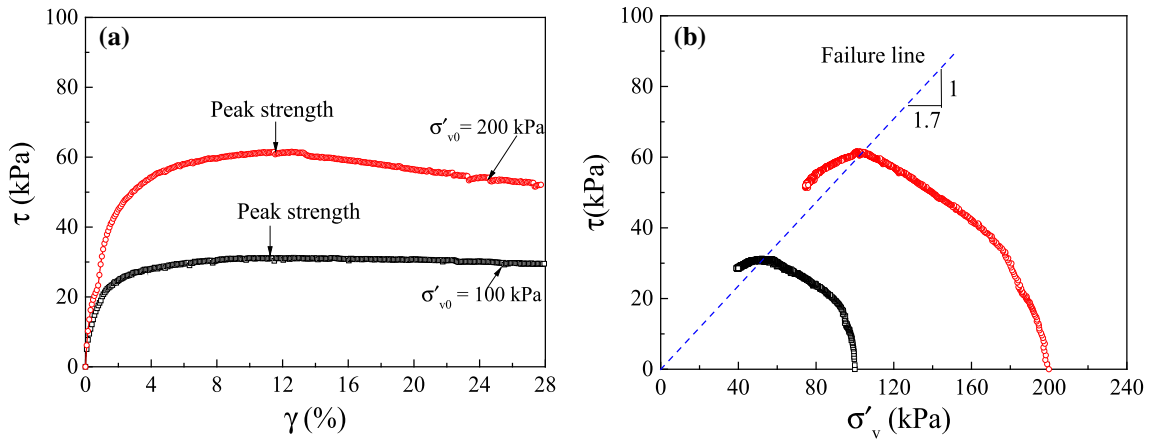
Fig. 5 Monotonic simple shear behavior of soft marine clay: **a** stress–strain relationships; **b** effective stress paths
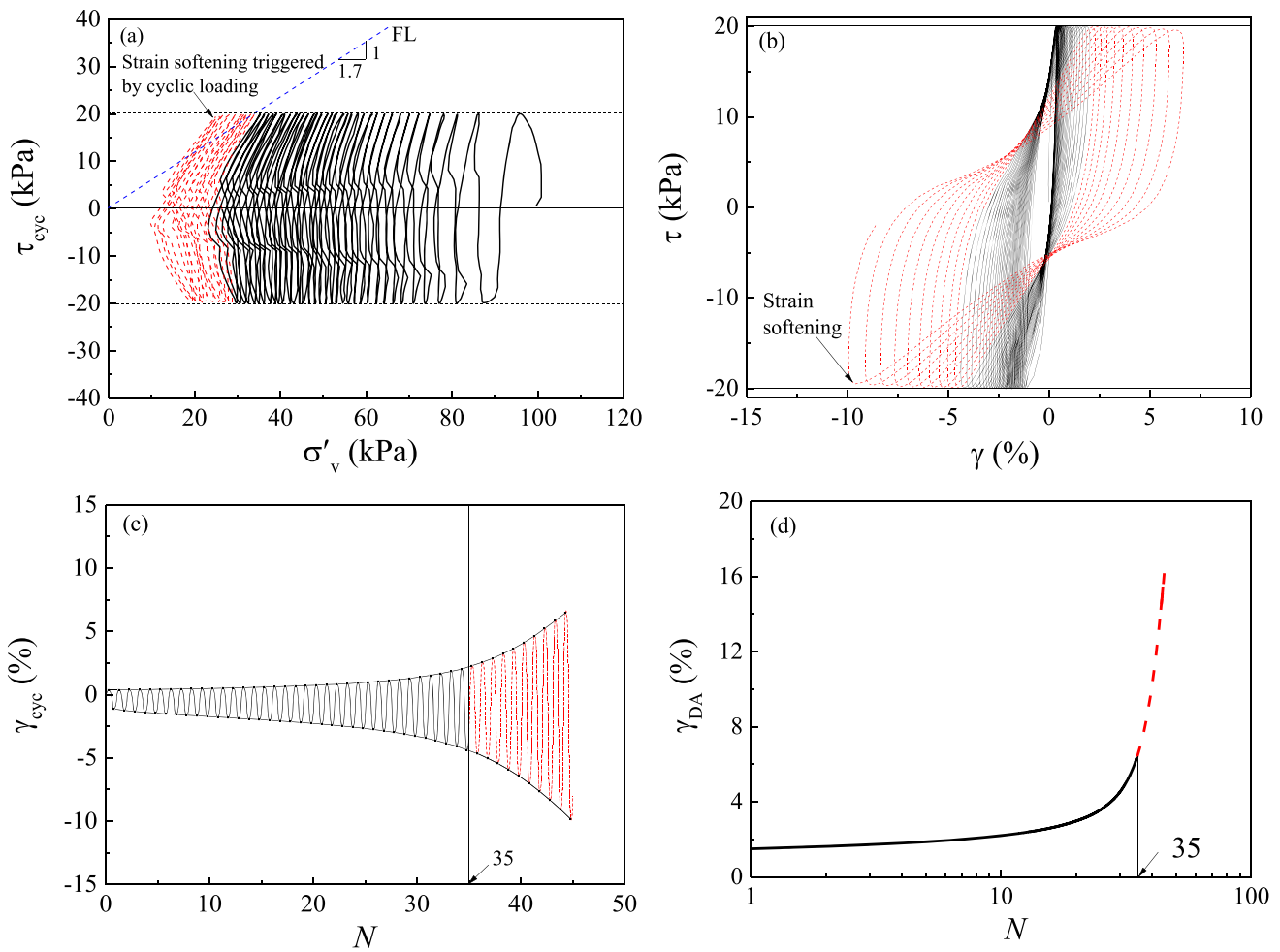

Fig. 6 Cyclic simple shear responses of soft marine clay under unidirectional loading (Test No. L2: CSR = 0.2): **a** effective stress path; **b** stress–strain curve; **c** cyclic shear strain; and **d** double-amplitude shear strain

During the subsequent cyclic loadings, the rate of decreasing σ'_v is reduced, and a "butterfly" stress path can be formed. The failure line (FL) defined in the monotonic shear tests is superimposed on the cyclic stress path, as shown in Fig. 6a. The moment when the effective stress path touches FL can be read from the figure as $N = 34.25$, which is generally rounded up to an integer, that is, $N = 35$. In the cyclic shearing following $N = 35$, the strain-

softening phenomenon characterized by the amplitude of the cyclic shear stress being below the target value of 20 kPa can be observed, as indicated by the dashed line in Fig. 6a. This phenomenon can also be observed in the hysteresis loop relating shear stress to shear strain, as shown in Fig. 6b. That is, the S-shaped loops are generally close to each other at the initial stage; however, they become more flattened and sparsely spaced when the number of shearing cycles $N > 35$. Figure 6c, d shows that the cyclic shear strain (γ_{cyc}) and the double-amplitude shear strain (γ_{DA}) increase significantly after the cyclic stress path reaches FL (i.e., $N > 35$). γ_{DA} is the sum of the maximum and minimum (in absolute value) shear strains obtained from each cycle of γ_{cyc} in Fig. 6c. A similar linkage between the cyclic behaviors observed above and the monotonic failure line has been widely reported for sandy soils [21, 30, 44, 46].

When multidirectional cyclic loadings are involved, that is, horizontal forces applied along both the x and y directions, it is more convenient to describe the cyclic behavior using the cyclic resultant shear stress ($\tau_{R\text{-}cyc}$) and cyclic resultant shear strain ($\gamma_{R\text{-}cyc}$), which are defined as:

$$\tau_{R-cyc} = \sqrt{\tau_{x-cyc}^2 + \tau_{y-cyc}^2} \tag{1}$$

$$\gamma_{R-cyc} = \sqrt{\gamma_{x-cyc}^2 + \gamma_{y-cyc}^2} \tag{2}$$

For the Series II test, typical results on the effective stress path, the stress–strain curve, and development of γ_{cyc} and $\gamma_{R\text{-}cyc}$ are presented in Fig. 7 for test No. C4, i.e., CSR = 0.2 and $\eta = 1$.

Similar to the observations made from the Series I test, the strain-softening phenomenon occurs when the effective stress path reaches the failure line. As can be seen from the dashed lines in Fig. 7, the amplitude of the resultant shear stress remains below the target value of 20 kPa; the hysteresis loops gradually become more inclined toward the horizontal axis, indicating a decrease in shear stiffness, and the cyclic shear strain increases drastically.

By maintaining the same CSR while reducing η to 0.7, an elliptical shear stress path can be formed, that is, Test No. E2 in the Series III test. The cyclic behavior is presented in Fig. 8. The trends of the effective stress paths, hysteresis loops, and development of shear strain over the number of cycles are the same as those depicted in Fig. 7. However, the number of cycles of the multidirectional shear stress when the effective stress path reaches the failure line is different between the two tests, that is, $N = 7$ in test No. C4 and $N = 11$ in E2. This difference is expected because the elliptical cyclic shear path is within the circular path, as shown in Fig. 4.

Figure 9 presents semi-log plots on γ_{DA} against N for the four tests in Series I. At a first glance, the γ_{DA}–log(N) plots

are nonlinear and separated by the different CSR values, a pattern similar to the results of previous works [10, 19]. γ_{DA} develops slowly at the initial stage of the cyclic loading. However, when the number of cycles reaches a certain value, the shear strain increases sharply, and the specimen will collapse. The number of cycles corresponding to the effective stress path touching FL (i.e., the critical number of cycles) can be determined from its plot, for instance, Figs. 6, 7, 8, which are marked with solid points on the γ_{DA} curve. The γ_{DA} corresponding to the critical number of cycles is located in the section where γ_{DA} increases sharply. Those shear strains can be connected to form a line with correlation coefficient (R^2) of 0.95 in the γ_{DA}–log(N) plot. For multidirectional cyclic shear loadings, the residual resultant shear strain $\gamma_{R\text{-}r}$ (i.e., γ_R at the end of each cycle) is plotted over the cycling number N, as shown in Fig. 10a, b for circular and elliptical stress paths, respectively. The trend of $\gamma_{R\text{-}r}$–log(N) is similar to those depicted in Fig. 9.

5 Cyclic shear strength

As mentioned in Introduction, the strength failure of a clay specimen can be established when the cyclic effective stress path reaches the failure line determined in monotonic tests [7, 24]. The cycling number when the effective stress path touches the failure line can be determined from its plot, as shown in Figs. 6, 7, 8. Therefore, the number of cycles associated with the solid points in Figs. 9 and 10 can be defined as the number of cycles to failure (N_f).

Using the cyclic shear stress ratio and the number of cycles to failure, a point can be determined in the CSR–log(N_f) coordinates. Figure 11 presents the points corresponding to test Series I (i.e., unidirectional loading) and II (multidirectional loading of circular stress path). In general, N_f decreases as CSR increases. For a given CSR, the required N_f under a circular stress path is less than that under a linear stress path, indicating that the failure is accelerated under multidirectional cyclic loadings. The discrete data points in the figure can be fitted using the following equation:

$$\text{CSR} = a\lambda(N_f)^{-b} \tag{3}$$

where a represents the intercept of the fitting curve to the vertical axis when $N_f = 1$ (i.e., a represents the CSR required for the failure of the specimen with only one cycle of loading), and b is the slope of the log(CSR)–log(N_f) plot. $a = 0.350$ and $b = 0.155$ can be determined for both the test series. The difference in shear strengths is reflected by parameter λ, whose value is 1 and 0.775 for the linear and circular shear stress paths, respectively. This observation
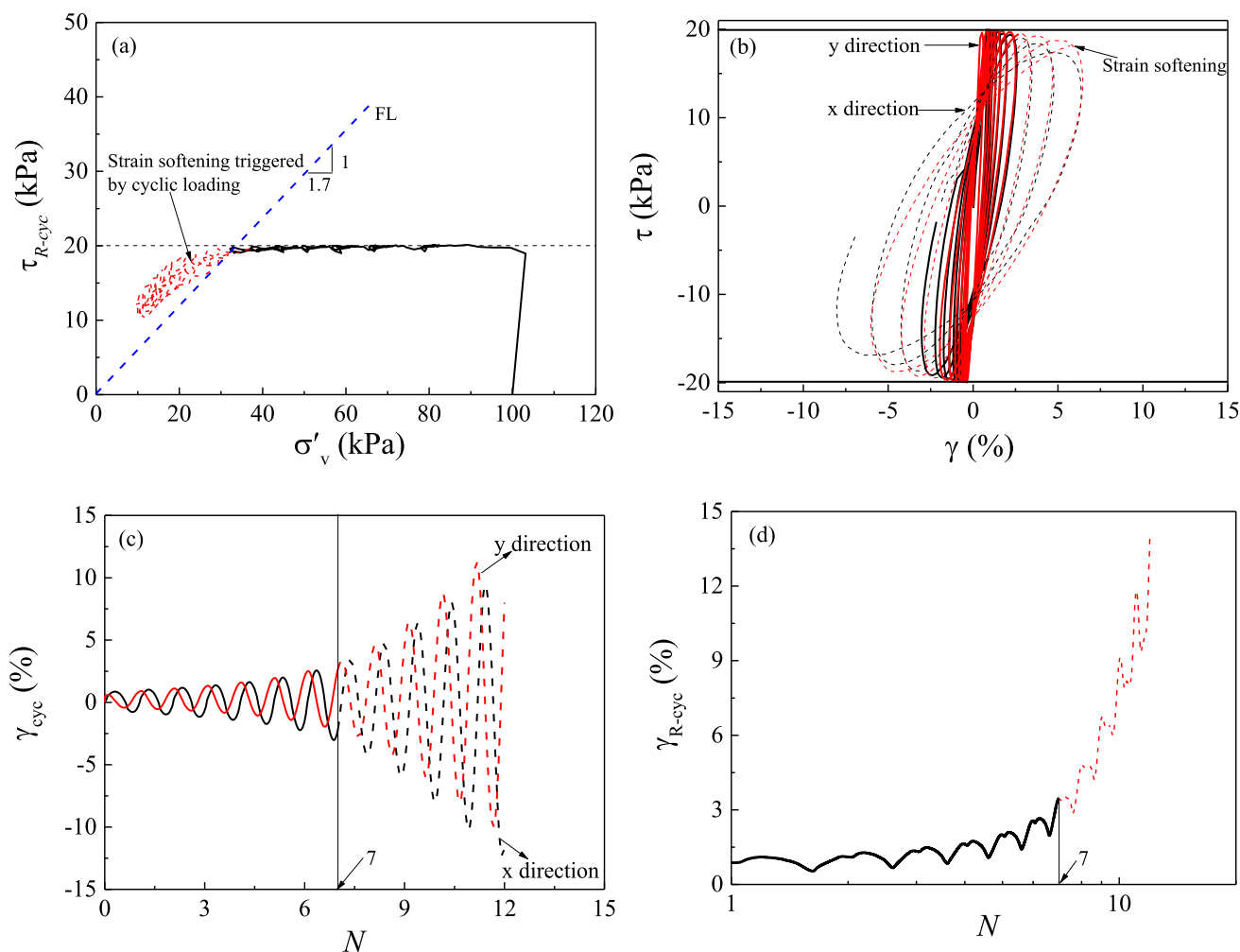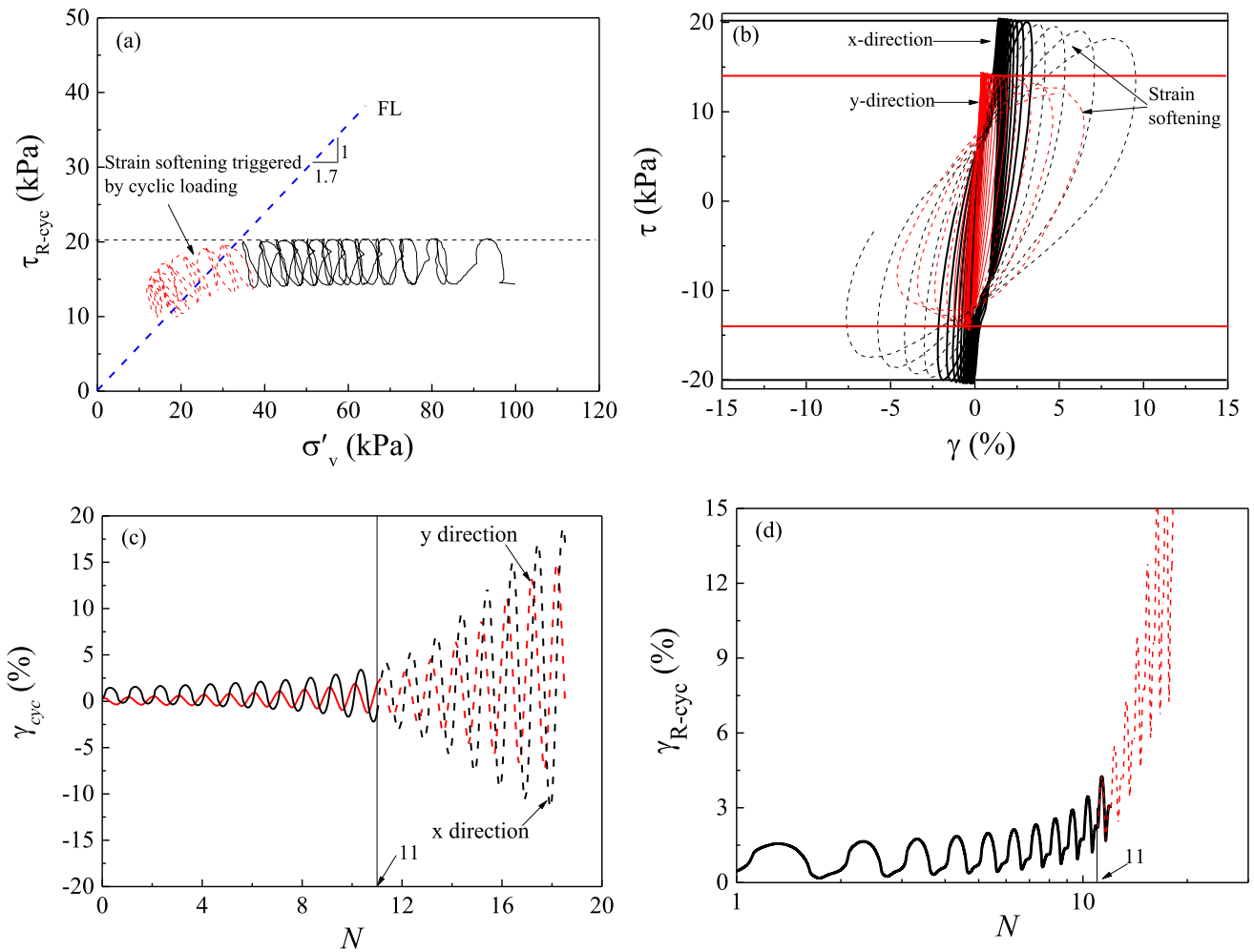
Fig. 7 Cyclic simple shear responses of soft marine clay under multidirectional loading (Test No. C4: CSR = 0.2 and η = 1): **a** effective stress path; **b** stress–strain curve; **c** cyclic shear strain; and **d** cyclic resultant shear strain

suggests that the cyclic strength of clay under a circular stress path is 0.775 times that under a linear stress path.

To study the effects of the elliptical stress path (i.e., $0 < \eta < 1$) on the cyclic shear strength, Fig. 12 presents the test data of Series III, which is presented as the amplitude ratio (η) between the two cyclic stresses versus the normalized number of cycles to failure $\left(N_f/N_f^{\eta=0}\right)$. $N_f^{\eta=0}$ denotes the number of cycles to failure under unidirectional cyclic shear tests, which can be predicted using Eq. (3). Notably, the four tests in Series III are of the same CSR = 0.2. In the semi-log plot of η against $N_f/N_f^{\eta=0}$, the four data points from test series III can be connected to a straight line. It can be observed that $N_f/N_f^{\eta=0}$ decreases with increasing η. To test the applicability of this linear relationship, data points corresponding to test series IV are added to Fig. 12, and a good match was observed. Thus, the linear relationship is independent of CSR in the $\eta -$

$\ln\left(N_f/N_f^{\eta=0}\right)$ plot. The line that reflects the effect of η on N_f is as follows:

$$\eta = \frac{1}{\ln(\lambda^{1/b})} \ln\left(N_f/N_f^{\eta=0}\right) \tag{4}$$

or

$$N_f/N_f^{\eta=0} = \lambda^{\eta/b} \tag{5}$$

Substituting Eq. (3) into Eq. (5), the following expression is obtained:

$$CSR = a\lambda^{\eta}(N_f)^{-b} \tag{6}$$

Equation (6) suggests that the cyclic strength of clay under multidirectional shearing (i.e., elliptic and circular stress paths) is λ^{η} times that under unidirectional shearing (i.e., linear stress path).

Fig. 8 Cyclic simple shear responses of soft marine clay under multidirectional loading (Test No. E2: CSR = 0.2 and η = 0.s7): **a** effective stress path; **b** stress–strain curve; **c** cyclic shear strain; and **d** cyclic resultant shear strain
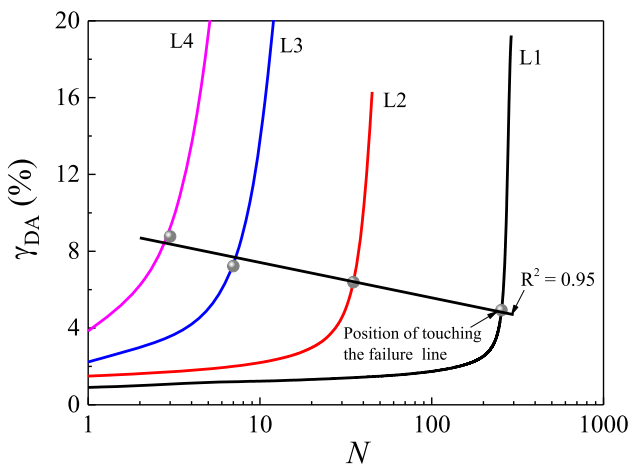
Fig. 9 Semilog plots of double-amplitude shear strain over number of cycles in unidirectional loading

6 Energy dissipation analysis of cyclic responses

The amount of dissipated energy represents the irreversible structural damage sustained by the soil skeleton during cyclic loading process [16, 17, 31]. The density of energy dissipation is represented by the area of the hysteresis loop relating the shearing stress to the shear strain, which can be calculated as follows:

$$W = \tau\gamma \tag{7}$$

In the multidirectional shear tests, Eq. (7) can be rewritten as

$$W = \tau_{R-cyc}\gamma_{R-cyc} \tag{8}$$

After substituting Eqs. (1) and (2) into Eq. (8), Eq. (8) can be rewritten as

$$W = \sqrt{(\tau_{x-cyc}\gamma_{x-cyc})^2 + (\tau_{y-cyc}\gamma_{y-cyc})^2 + \tau_{y-cyc}\gamma_{x-cyc} + \tau_{x-cyc}\gamma_{y-cyc}} \qquad (9)$$

where the two bracketed terms can be evaluated by calculating the area of the hysteresis loop in the x- and y-directions. Because the stress and strain directions of the last two terms are perpendicular to each other, there is no energy dissipation (i.e., the values of the last two terms are zero). The evaluation process is schematized in Fig. 13, where the area of the hysteresis loop is discretized into a series of load increments, that is,

$$W_{x,y} = \sum_{i=1}^{n-1} \frac{1}{2}(\tau_{i+1} + \tau_i)(\gamma_{i+1} - \gamma_i) \qquad (10)$$

where n denotes the total number of increments; τ_i and γ_i represent the shear stress and strain of the ith increment, respectively.

6.1 Energy dissipation for cyclic failure

The development of the energy dissipation (W) with the number of cycles is presented in Fig. 14. The accumulation of W with the number of cycles shows a similar pattern to the development of $\gamma_{R\text{-}r}$ (see Fig. 10), that is, W develops slowly at the initial stage of cyclic loading, and it increases sharply when the number of cycles reaches a certain value. The accumulation of W is highly dependent on CSR and η. When CSR varies and η remains constant, as shown in Fig. 14a, the energy dissipated during the first loading cycle (i.e., $N = 1$) increases with increasing CSR. With increasing N, the gap between neighboring W–
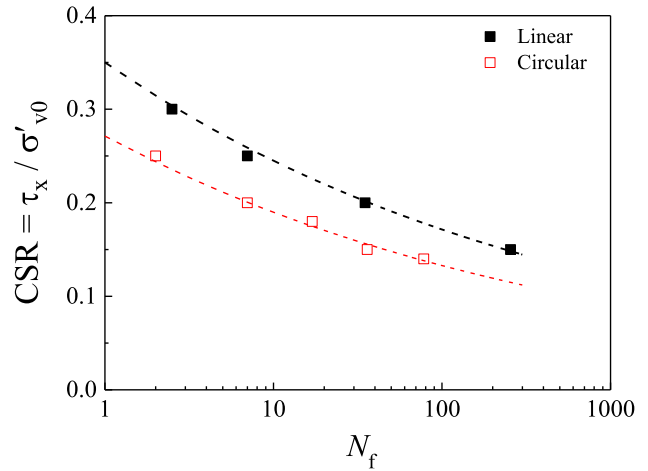
Fig. 11 Number of cycles to failure (N_f) against CSR under linear and circular stress paths

log(N) curves increases before the failure state is reached. When η varies and CSR remains constant, a similar observation can be made, as shown in Fig. 14b. The vertical coordinate of the solid points in Fig. 14 represents the energy dissipation when cyclic failure occurs in the specimen, which is denoted as W_f, and it is dependent on N_f or cyclic stress amplitude.

Certain test cases in Table 2 show the same or similar number of cycles to failure even though the stress paths are different, for example, $N_f = 7$ for cases L3, C4, and E5, and
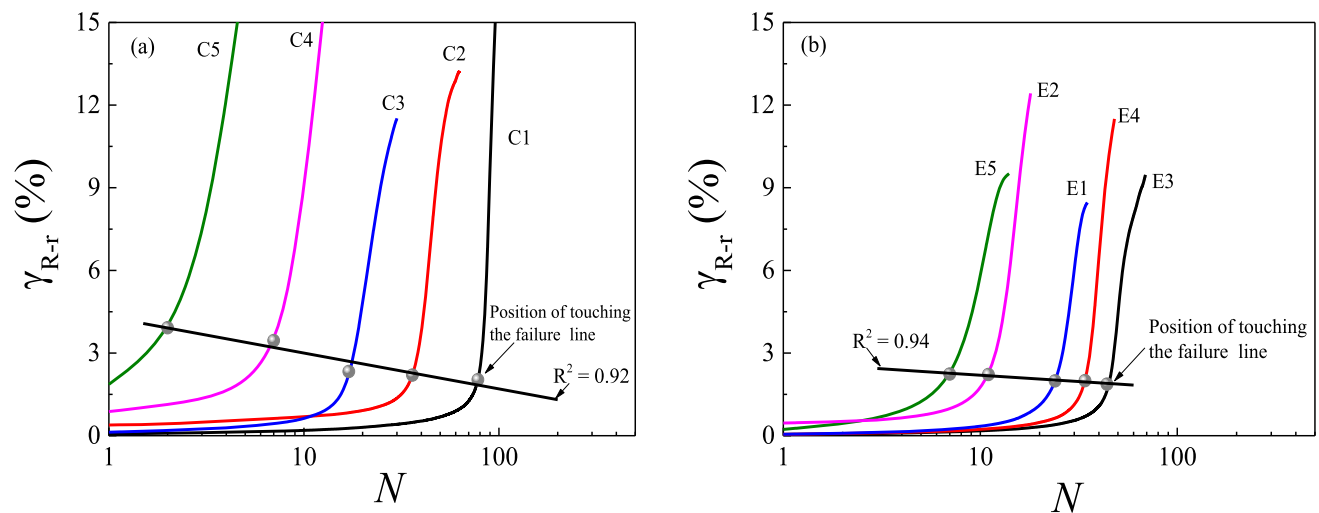

Fig. 10 Semi-log plots of residual resultant shear strain over number of load cycles in multidirectional loading: **a** circular stress path; **b** elliptical stress path
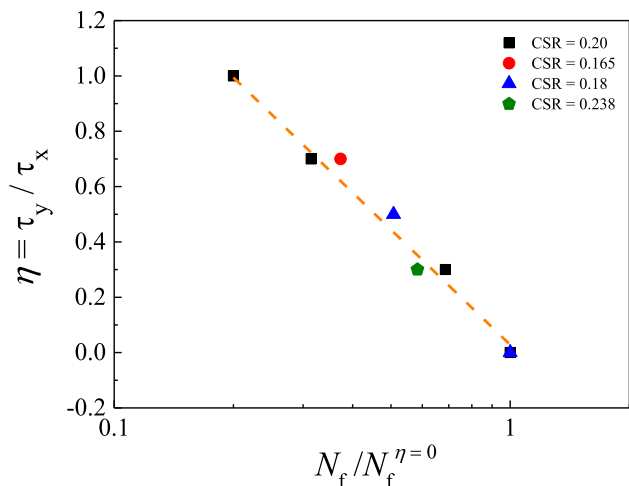
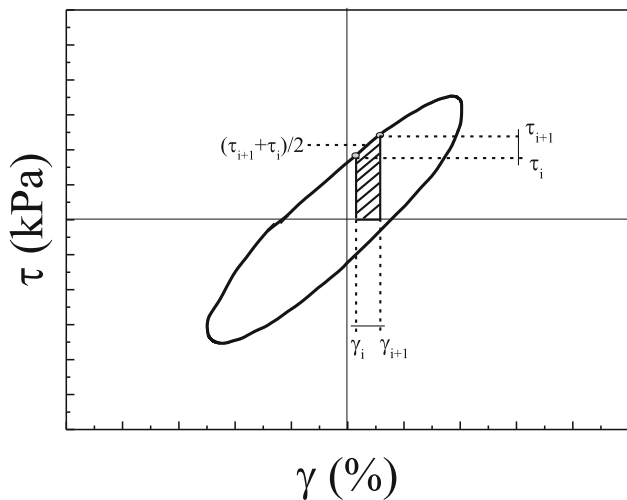**Fig. 12** Semi-log plot of normalized number of cycles to failure $N_f/N_f^{\eta=0}$ over amplitude ratio η
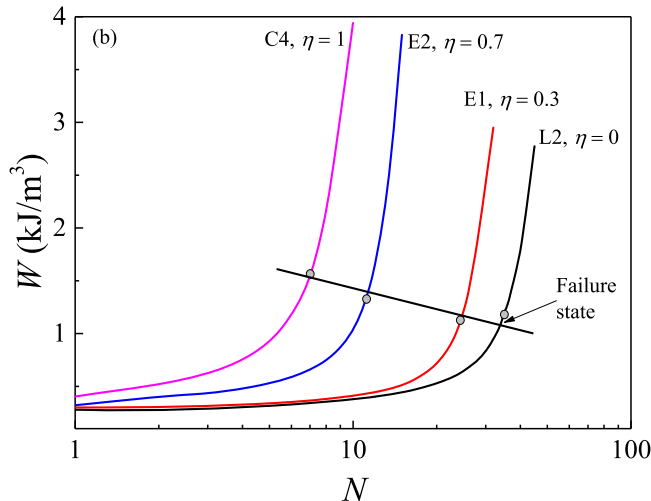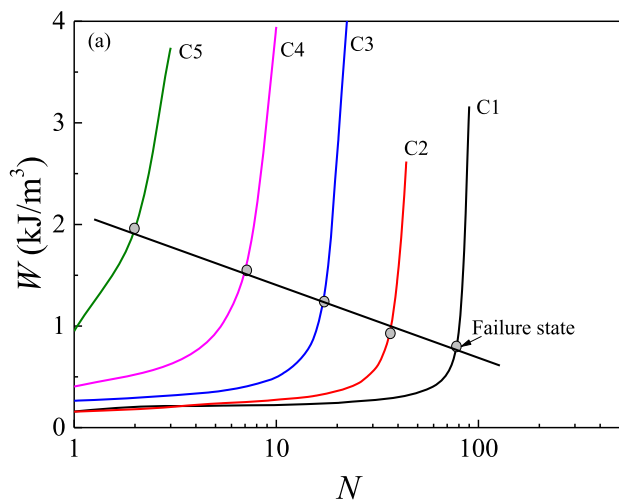

Fig. 13 Schematic of evaluation of hysteresis loop area

$N_f \approx 35$ for cases L2, C2, and E4. For these cases, the accumulations of W are drawn in Fig. 15 for the increasing number of cycles N. It is observed that the W–log(N) curves associated with the same/similar N_f almost overlap. Figure 16 summarizes the results of the energy dissipation for cyclic failure (W_f) against the number of cycles to failure (N_f). Notably, all data points converge around a curve regardless of the stress paths, which implies that the coupling effects of CSR and η on the cyclic strength can be uniformly interpreted utilizing the concept of energy dissipation.

6.2 Pore water pressure analysis based on energy dissipation

The pore water pressure (Δu) of soft clay is important for understanding its cyclic behavior and evaluating the effective stresses [25, 32, 42]. The development of Δu with increasing cycling numbers is presented in Fig. 17 for test Series III. The four tests utilize the same CSR and different values of η. The accumulation rate of Δu increases with η. For instance, the specimen requires 24 cycles to develop $\Delta u = 60$ kPa when $\eta = 0$, whereas it only takes 6 cycles to reach the same Δu for cyclic loading with $\eta = 1$. The development trends of Δu of the specimens associated with different η share the same power-law pattern when the loading cycle increases. Δu can be divided into transient and residual components, as shown in Fig. 17. The former is equal to the change in the total stress, and thus, it oscillates with the cycling load. The latter is derived at the end of each stress cycle, that is when the cyclic shear stress becomes zero [34]. Thus, the residual pore water pressure (Δu_r) reflects the irrecoverable pore water pressure accumulation, which directly alters the effective stress and, subsequently, the soil strength.
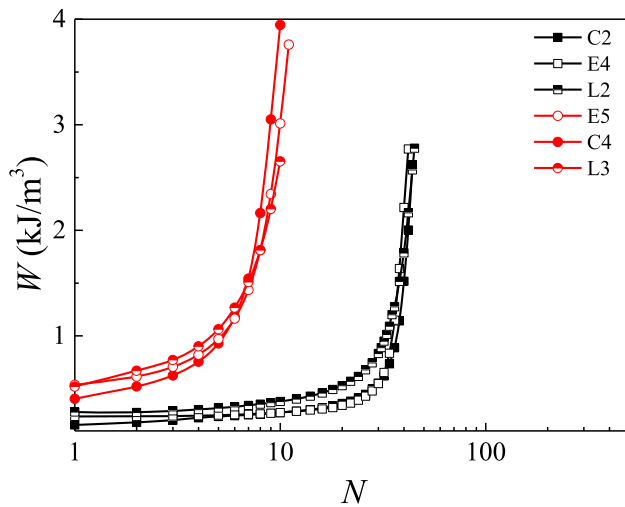

Fig. 14 Semi-log plots of energy dissipation (W) over number of cycles (N): **a** test Series II; **b** test Series III

Fig. 15 Comparing the accumulation of energy dissipation (W) with the number of cycles (N) under a similar number of cycles to failure (N_f)
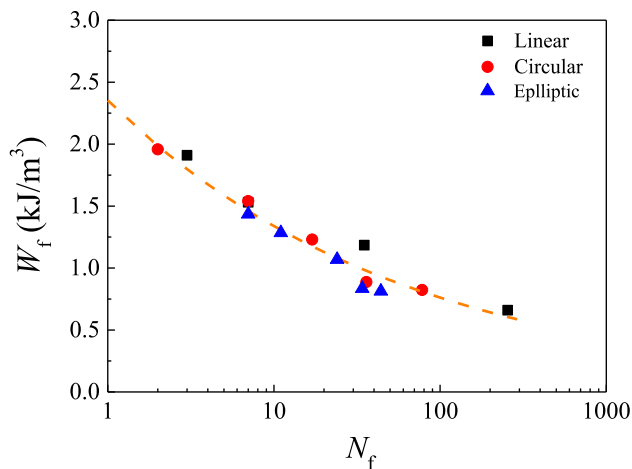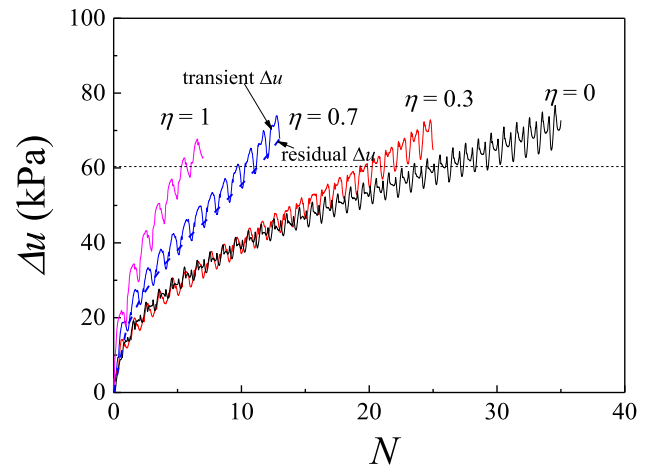

Fig. 17 Development of excess pore water pressure with respect to number of cycles under CSR = 0.2

bounded by two dashed lines. This demonstrates that the normalized pore pressure–energy relationship of soft clay is independent of the cyclic shear stress path.

7 Discussion on criteria for cyclic failure

As mentioned in Introduction, different criteria exist in the literature for judging the cyclic failure of clay specimens. Here, we focus on two types of criteria: one is failure–line based [7, 24], that is, cyclic failure occurs when the ever-developing effective stress path touches the failure line, and the other is inflection based [19] because the clay specimens generally collapse in a relatively short period once the shear strain is larger than that corresponding to the inflection of the shear strain–number of cycle curves. To determine the inflection, the initial and later trends of the curve are represented by two tangents, as shown in Fig. 20. The two tangents intersect at an angle, the bisector of which crosses the strain curve; the crossing point is the inflection. Similar methods for determining the inflection of curve can be found in the work of Ansal and Erken [6]. The strain obtained from the inflection is referred to as failure strain. Evidently, the first criterion is rooted in the physical mechanism of material strength, whereas the latter is characterized by phenomenological laboratory observations. To compare the two criteria, four inflections are identified and superimposed in Fig. 9, which contains solid points representing cyclic failure, as determined by the failure line-based criterion. The four inflections in Fig. 20 are connected to form a straight dashed line, which is separate from the solid line.

With the number of cycles to failure (N_f) determined from the inflection-based criteria, the data presented in Figs. 12, 16, and 19 can be processed in the same manner,
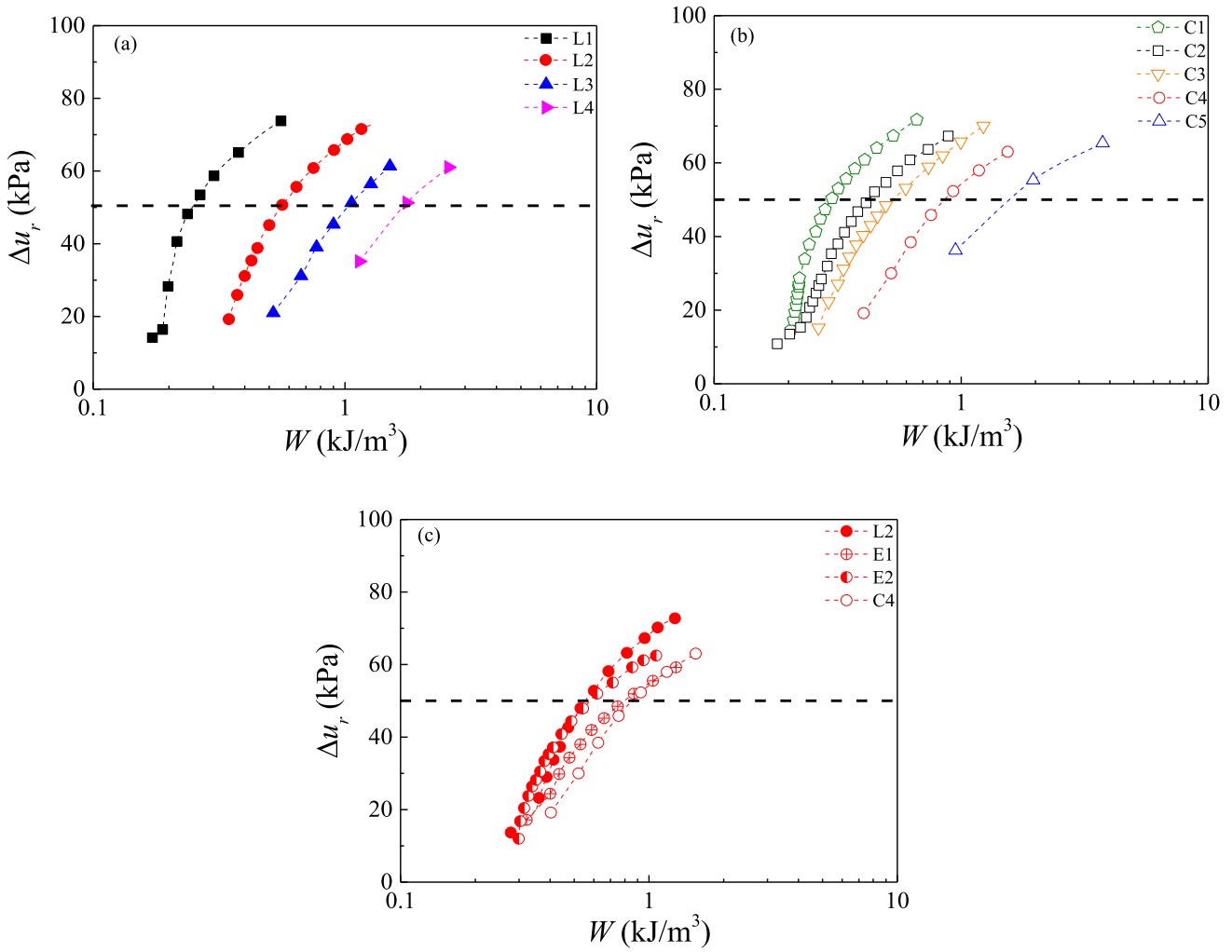

Fig. 16 Energy dissipation for failure (W_f) against number of cycles to failure (N_f)

Δu_r has been studied from the viewpoint of energy dissipation [31, 33, 45]. Figure 18 presents the variation in Δu_r versus energy dissipation before specimen failure. The Δu_r–log(W) plots associated with different stress paths (i.e., combinations of CSR and η) are convex to the vertical axis, that is, the developing rate of Δu_r changes from high to low with increasing energy dissipation. Figure 18 shows that the energy dissipation (W) increases with increasing CSR and η for a particular lever of power water pressure accumulation (e.g., Δu_r = 50 kPa).

The development of the residual pore water pressure can be normalized by dividing the residual pore water pressure at failure, that is, $\Delta u_r / \Delta u_{r\text{-}f}$. The accumulation of energy dissipation can be processed in the same manner, that is, W/W_f. The processed data from all the test cases in Table 2 are presented in Fig. 19, which falls within a narrow strip

Fig. 18 Residual pore pressure against dissipated energy: **a** test Series I; **b** test Series II; **c** test Series III
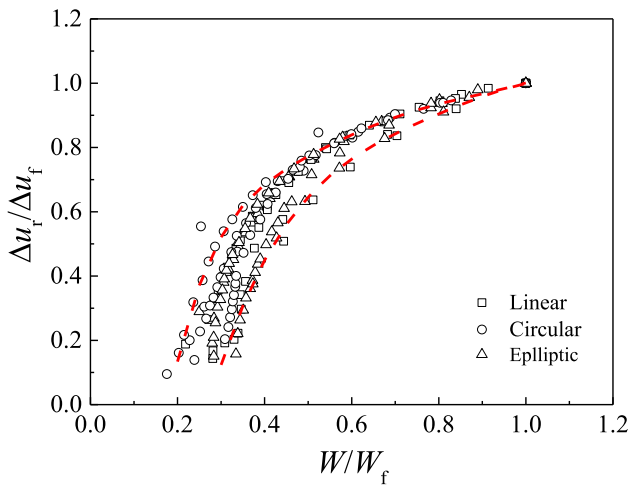

Fig. 19 Relationship between normalized residual pore water pressure and dissipated energy
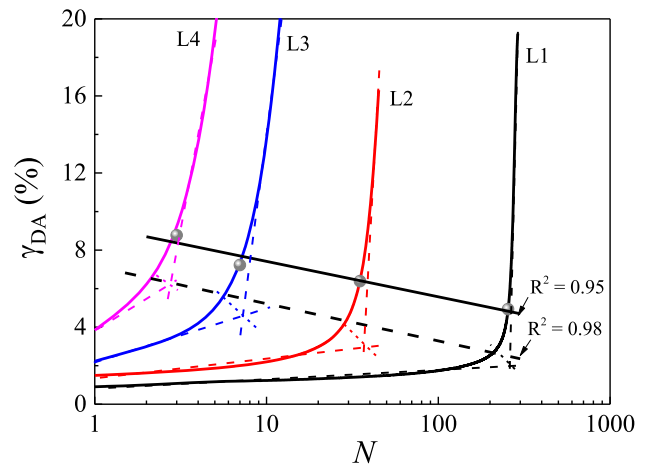

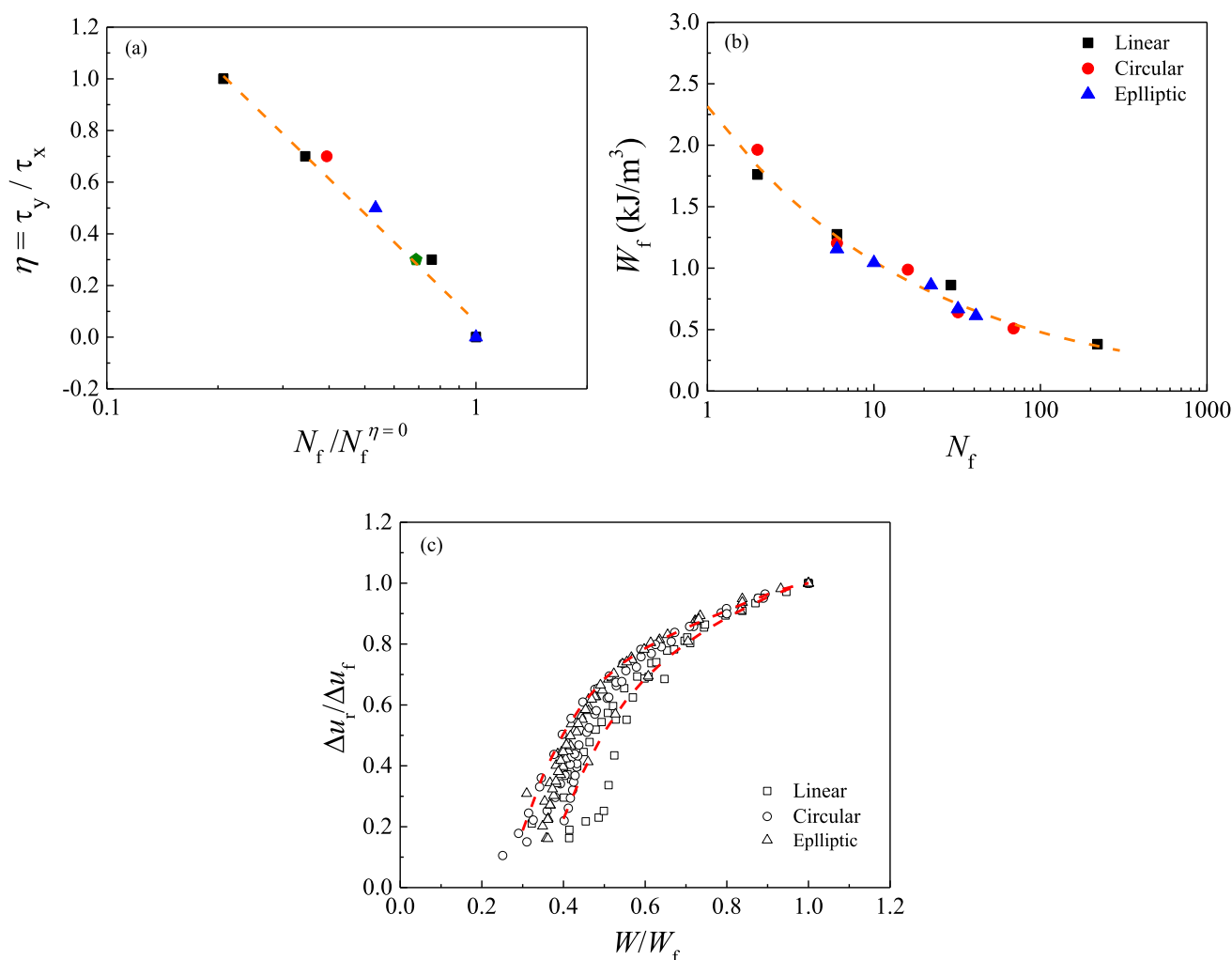**Fig. 20** Comparison on failure line and inflection-based criteria for assessing cyclic failure of clay specimens

Fig. 21 Influences of failure criterion based on inflection points on undrained cyclic behavior of clay: **a** η against $N_f/N_f^{\eta=0}$; **b** W_f against N_f; **c** $\Delta u_r/\Delta u_f$ against W/W_f

as shown in Fig. 21. Notably, the distribution patterns of the scattered data points as well as the fitting/bounding curves are largely the same as those in Figs. 12, 16, and 19, which indicates that the linear dependence of N_f on the η, the stress path-independent relationship between W_f and N_f, and the correlation between $\Delta u_r/\Delta u_f$ and W/W_f are not affected by the failure criteria adopted.

8 Conclusions

In this study, the cyclic responses of marine soft clay subjected to multidirectional cyclic shear stresses were investigated using a variable-direction dynamic cyclic shear system. Four series of laboratory tests with different loading amplitudes (i.e., the cyclic stress ratio (CSR)) and patterns of stress path (i.e., the linear, circular, and elliptical paths governed by the amplitude ratio (η)) were

designed and conducted. The effective stress path, shear strain, cyclic strength, and pore water pressure were presented and analyzed. Moreover, using the concept of dissipated energy, the undrained cyclic strength and pore water pressure generation of soft clay were studied. The main conclusions are as:

(1) After the cyclic effective stress path reaches the failure line determined in monotonic tests, a strain-softening phenomenon can be observed. It is more pronounced for multidirectional shear loading than for unidirectional loading.

(2) An empirical formula is established to predict the cyclic strength of soft clay under different shear stress paths. In particular, it is found that the cyclic strength of clay subjected to multidirectional cyclic shear stresses (i.e., circular and elliptical stress paths) is 0.775^{η} times that under unidirectional shear stresses (i.e., linear stress path).

(3) The accumulation of dissipated energy with increasing loading cycles is influenced by CSR and η, which is essentially related to the number of cycles to failure. The coupling effects of CSR and η on cyclic strength can be uniformly interpreted through the concept of energy dissipation.

(4) By establishing the normalized energy–residual pore pressure relationship, a unified interpretation method is proposed, whereby the residual pore pressure is uniquely related to the dissipated energy, irrespective of the cyclic stress amplitude and stress path.

Data availability The data underlying this article will be shared on reasonable request to the corresponding author.

Declarations

Conflict of interest The authors have no conflicts of interest to declare that are relevant to the content of this article.

References

1. Airey DW, Wood DM (1986) Pore pressures in simple shear. Soils Found 26(2):91–96
2. Airey DW, Wood DM (1987) An evaluation of direct simple shear tests on clay. Soils and Géotechnique 37(1):25–35
3. Al-Tarhouni M, Simms P, Sivathayalan S (2011) Cyclic behaviour of reconstituted and desiccated–rewet thickened gold tailings in simple shear. Can Geotech J 48(7):1044–1060
4. Andersen KH (2009) Bearing capacity under cyclic loading — offshore, along the coast, and on land. The 21st Bjerrum Lecture presented in Oslo, 23 November 2007. Can Geotech J 46(5):513–535
5. Andersen KH (2015) Cyclic soil parameters for offshore foundation design. in: Proceeding of International Symposium on Frontiers in Offshore Geotechnics: ISFOG, Oslo, Norway: 5–82
6. Ansal AM, Erken A (1989) Undrained behavior of clay under cyclic shear stresses. J Geotech Eng 115(7):968–983
7. Azzouz AS, Malek AM, Baligh MM (1989) Cyclic behavior of clays in undrained simple shear. J Geotech Eng 115(5):637–657
8. Dyvik R, Berre T, Lacasse S (1987) Comparison of truly undrained and constant volume direct simple shear tests. Géotechnique 37(1):3–10
9. Figueroa JL, Saada AS, Liang L, Dahisaria NM (1994) Evaluation of soil liquefaction by energy principles. J Geotech Eng 120(9):1554–1569
10. Gu C, Wang J, Cai Y, Yang Z, Gao Y (2012) Undrained cyclic triaxial behavior of saturated clays under variable confining pressure. Soil Dyn Earthq Eng 40:118–128
11. Guo L, Jin H, Wang J, Shi L (2020) Undrained monotonic shear behavior of marine soft clay after long-term cyclic loading. Marine Georesources Geotechnol 38(7):854–866
12. Guo L, Wang J, Cai Y, Liu H, Gao Y, Sun H (2013) Undrained deformation behavior of saturated soft clay under long-term cyclic loading. Soil Dyn Earthq Eng 50:28–37
13. Hu X, Zhang Y, Guo L, Wang J, Cai Y, Fu H, Cai Y (2018) Cyclic behavior of saturated soft clay under stress path with bidirectional shear stresses. Soil Dyn Earthq Eng 104:319–328
14. Hyodo M, Hyde AFL, Yamamoto Y, Fujii T (1999) Cyclic Shear strength of undisturbed and remoulded marine clays. Soils Found 39(2):45–58
15. Jin H, Guo L (2021) Effect of phase difference on the liquefaction behavior of sand in multidirectional simple shear tests. J Geotech Geoenviron Eng 147(12):06021015
16. Kokusho T (2013) Liquefaction potential evaluations: energy-based method versus stress-based method. Can Geotech J 50(10):1088–1099
17. Law KT, Cao YL, He GN (1990) An energy approach for assessing seismic liquefaction potential. Can Geotech J 27(3):320–329
18. Lee KL (1979) Cyclic strength of a sensitive clay of eastern Canada. Can Geotech J 16(1):163–176
19. Li L-L, Dan H-B, Wang L-Z (2011) Undrained behavior of natural marine clay under cyclic loading. Ocean Eng 38(16):1792–1805
20. Li Y, Yang Y, Yu H-S, Roberts G (2017) Monotonic direct simple shear tests on sand under multidirectional loading. Int J Geomech 17(1):04016038
21. Li Y, Yang Y, Yu H-S, Roberts G (2017) Correlations between the stress paths of a monotonic test and a cyclic test under the same initial conditions. Soil Dyn Earthq Eng 101:153–156
22. Liang L, Figueroa JL, Saada AS (1995) Liquefaction under random loading: unit energy approach. J Geotech Eng 121(11):776–781
23. Liu FY, Chen L, Hu XQ, Wang J, Cai Y (2018) Cyclic simple shear tests on saturated soft clay subjected to ellipse stress path. China J Highw Transp 32(2):218–225
24. Malek AM, Azzouz AS, Baligh MM, Germaine JT (1989) Behavior of foundation clays supporting compliant offshore structures. J Geotech Eng 115(5):615–636
25. Matasovic N, Vucetic M (1995) Generalized cyclic-degradation pore-pressure generation model for clays. J Geotech Eng 121(1):33–42
26. Matsuda H, Nhan TT, Ishikura R (2013) Excess pore water pressure accumulation and recompression of saturated soft clay subjected to uni-directional and multi-directional cyclic simple shears. J Earthq Tsunami 07(04):1250027
27. Matsuda H, Thanh Nhan T, Ishikura R (2013) Prediction of excess pore water pressure and post-cyclic settlement on soft clay induced by uni-directional and multi-directional cyclic shears as a function of strain path parameters. Soil Dyn Earthq Eng 49:75–88
28. Nemat-Nasser S, Shokooh A (1979) A unified approach to densification and liquefaction of cohesionless sand in cyclic shearing. Can Geotech J 16(4):659–678

29. Nikitas G, Vimalan NJ, Bhattacharya S (2016) An innovative cyclic loading device to study long term performance of offshore wind turbines. Soil Dyn Earthq Eng 82:154–160

30. Pan K, Cai YQ, Yang ZX, Pan XD (2019) Liquefaction of sand under monotonic and cyclic shear conditions: Impact of drained preloading history. Soil Dyn Earthq Eng 126:105775

31. Pan K, Yang ZX (2020) Evaluation of the liquefaction potential of sand under random loading conditions: Equivalent approach versus energy-based method. J Earthq Eng 24(1):59–83

32. Paul M, Sahu RB, Banerjee G (2015) Undrained pore pressure prediction in clayey soil under cyclic loading. Int J Geomech 15(5):04014082

33. Polito C, Green RA, Dillon E, Sohn C (2013) Effect of load shape on relationship between dissipated energy and residual excess pore pressure generation in cyclic triaxial tests. Can Geotech J 50(11):1118–1128

34. Polito CP, Green RA, Lee J (2008) Pore pressure generation models for sands and silty soils subjected to cyclic loading. J Geotech Geoenviron Eng 134(10):1490–1500

35. Rudolph C, Bienen B, Grabe J (2014) Effect of variation of the loading direction on the displacement accumulation of large-diameter piles under cyclic lateral loading in sand. Can Geotech J 51(10):1196–1206

36. Su D, Li XS (2008) Impact of multidirectional shaking on liquefaction potential of level sand deposits. Géotechnique 58(4):259–267

37. Su D, Li JH (2013) Three-dimensional finite element study of a single pile response to multidirectional lateral loadings incorporating the simplified state-dependent dilatancy model. Comput Geotech 50:129–142

38. Suazo G, Fourie A, Doherty J, Hasan A (2016) Effects of confining stress, density and initial static shear stress on the cyclic shear response of fine-grained unclassified tailings. Géotechnique 66(5):401–412

39. Su D (2012) Resistance of short, stiff piles to multidirectional lateral loadings. Geotech Test J 35(2):103840

40. Wang Y, Gao Y, Guo L, Cai Y, Li B, Qiu Y, Mahfouz AH (2017) Cyclic response of natural soft marine clay under principal stress rotation as induced by wave loads. Ocean Eng 129:191–202

41. Wang J, Guo L, Cai Y, Xu C, Gu C (2013) Strain and pore pressure development on soft marine clay in triaxial tests with a large number of cycles. Ocean Eng 74:125–132

42. Wang J, Wu L, Cai Y, Guo L, Du Y, Gou C, Ni J, Gao Z (2021) Monotonic and cyclic characteristics of K0-Consolidated saturated soft clay under a stress path involving a variable confining pressure. Acta Geotech 16(4):1161–1174

43. Wang J, Zhuang H, Guo L, Cai Y, Li M, Shi L (2021) Secondary compression behavior of over-consolidated soft clay after surcharge preloading. Acta Geotech 17:1009–1016. https://doi.org/10.1007/s11440-021-01276-9

44. Yang ZX, Pan K (2017) Flow deformation and cyclic resistance of saturated loose sand considering initial static shear effect. Soil Dyn Earthq Eng 92:68–78

45. Yang ZX, Pan K (2018) Energy-based approach to quantify cyclic resistance and pore pressure generation in anisotropically consolidated sand. J Mater Civ Eng 30(9):04018203

46. Yang J, Sze HY (2011) Cyclic behaviour and resistance of saturated sand under non-symmetrical loading conditions. Géotechnique 61(1):59–73

47. Yasuhara K, Yamanouchi T, Hirao K (1982) Cyclic strength and deformation of normally consolidated clay. Soils Found 22(3):77–91